THE JOURNAL OF BIOLOGICAL CHEMISTRY
Vol. 280, No. 10, Issue of March 11, pp. 9272–9282, 2005

Printed in U.S.A.

Bass Hepcidin Synthesis, Solution Structure, Antimicrobial Activities and Synergism, and *in Vivo* Hepatic Response to Bacterial Infections*[S]

Received for publication, September 29, 2004, and in revised form, November 11, 2004
Published, JBC Papers in Press, November 16, 2004, DOI 10.1074/jbc.M411154200

Xavier Lauth‡§, Jeffrey J. Babon¶, Jason A. Stannard§, Satendra Singh‖, Victor Nizet‡, James M. Carlberg§, Vaughn E. Ostland§, Michael W. Pennington‖, Raymond S. Norton¶, and Mark E. Westerman§**

From the ‡Department of Pediatrics, University of California San Diego, School of Medicine, San Diego, California 92093, ¶The Walter & Eliza Hall Institute of Medical Research, 1G Royal Parade, Parkville, Victoria 3050, Australia, §Kent SeaTech Corp., San Diego, California 92121, and ‖BACHEM Biosciences Inc., King of Prussia, Pennsylvania 19406

Bass hepcidin was purified from the gill of hybrid striped bass (*Morone chrysops* × *Morone saxatilis*) based on antimicrobial activity against *Escherichia coli*. This 21-amino acid peptide has 8 cysteines engaged in 4 disulfide bonds and is very similar to human hepcidin, an antimicrobial peptide with iron regulatory properties. To gain insight into potential role(s) of bass hepcidin in innate immunity in fish, we synthesized the peptide, characterized its antimicrobial activities *in vitro*, determined its solution structure by NMR, and quantified hepatic gene expression *in vivo* following infection of bass with the fish pathogens, *Streptococcus iniae* or *Aeromonas salmonicida*. Its structure is very similar to that of human hepcidin, including the presence of an antiparallel β-sheet, a conserved disulfide-bonding pattern, and a rare vicinal disulfide bond. Synthetic bass hepcidin was active *in vitro* against Gram-negative pathogens and fungi but showed no activity against key Gram-positive pathogens and a single yeast strain tested. Hepcidin was non-hemolytic at microbicidal concentrations and had lower specific activity than moronecidin, a broad spectrum, amphipathic, α-helical, antimicrobial peptide constitutively expressed in bass gill tissue. Good synergism between the bacterial killing activities of hepcidin and moronecidin was observed *in vitro*. Hepcidin gene expression in bass liver increased significantly within hours of infection with Gram-positive (*S. iniae*) or Gram-negative (*A. salmonicida*) pathogens and was 4–5 orders of magnitude above base-line 24–48 h post-infection. Our results suggest that hepcidin plays a key role in the antimicrobial defenses of bass and that its functions are potentially conserved between fish and human.

In vertebrates from fish to human, the hepcidins form a new gene family of immune-inducible, liver-expressed, and cysteine-rich peptides (1–4). Human hepcidin, also known as liver-expressed antimicrobial peptide, was initially purified as a 25-amino acid peptide from urine and plasma ultrafiltrates during screenings for proteins/peptides with antimicrobial activity (1, 2). Expressed sequence tag data base searches revealed related hepcidin sequences among various species of fish; this observation was confirmed by the characterization of a new hepcidin peptide that was purified from the gill tissues of hybrid striped bass (HSB[1]; *Morone chrysops* × *Morone saxatilis*) based on its antimicrobial activity against an *Escherichia coli* strain (5, 6). Like human hepcidin, the bass hepcidin peptide possesses 8 cysteines involved in 4 disulfide bonds and was predominantly expressed in the liver. Bass hepcidin was co-purified from the gill of HSB with another antimicrobial peptide, moronecidin, which was found to have very potent, broad spectrum antimicrobial activity (5).

In addition to antimicrobial activities, mammalian hepcidins were found to play an essential role in iron homeostasis. This was first suggested in studies using subtractive cloning approaches in mice subjected to dietary iron overload (7). Hepcidin gene expression was up-regulated under iron overload conditions, and disruption of the hepcidin gene led to accumulation of iron in the liver and pancreas, as well as iron depletion in resident macrophages. This pattern closely paralleled the iron distribution pattern seen in cases of hereditary hemochromatosis in humans (8). In another study, overexpression of hepcidin in transgenic mouse pups induced profound anemia and postpartum mortality (9). These and other observations led to the hypothesis that elevated levels of hepcidin limit dietary iron uptake in duodenal enterocytes and block the release of iron by macrophages, making hepcidin a key regulator/hormone of iron homeostasis in higher vertebrates (10). A critical role for hepcidin in human iron regulation was recently corroborated by association of deleterious mutations in the hepcidin

* This work was supported by National Science Foundation Grants DMI-0215093 and DMI-0349772. The costs of publication of this article were defrayed in part by the payment of page charges. This article must therefore be hereby marked "*advertisement*" in accordance with 18 U.S.C. Section 1734 solely to indicate this fact.

The atomic coordinates and structure factors (code 1S6W) have been deposited in the Protein Data Bank, Research Collaboratory for Structural Bioinformatics, Rutgers University, New Brunswick, NJ (http://www.rcsb.org/).

[S] The on-line version of this article (available at http://www.jbc.org) contains Figs. A1–S5 and Table S1.

** To whom correspondence should be addressed: Kent SeaTech Corp., 11125 Flintkote Ave., Ste. J, San Diego, CA 92121. Tel.: 858-452-5765; Fax: 858-452-0075; E-mail: mwesterman@kentseatech.com.

[1] The abbreviations used are: HSB, hybrid striped bass; AMP, antimicrobial peptide; CFU, colony-forming units; Me_2SO, dimethyl sulfoxide; DQF-COSY, double quantum filtered correlation spectroscopy; FIC, fractional inhibition concentration; Fmoc, 9-fluorenylmethyloxycarbonyl; HSQC, heteronuclear single quantum coherence; IL, interleukin; IP, intraperitoneal; LB, Luria broth; MALDI-TOF, matrix-assisted laser desorption time of flight spectrometry; MBC, minimum bactericidal concentration; MeCN, acetonitrile; MIC, minimum inhibitory concentration; NOE, nuclear Overhauser effect; NOESY, nuclear Overhauser and exchange spectroscopy; PBS, phosphate-buffered saline; PDB, potato dextrose broth; RP-HPLC, reversed phase-high pressure liquid chromatography; RT, reverse transcription; THB, Todd Hewitt Broth; TOCSY, total correlation spectroscopy; r.m.s.d., root mean square deviation.

gene in several consanguine families with severe juvenile hemochromatosis (11, 12) and with demonstration of abnormal hepcidin gene expression levels in patients with other genetic variants of this disease (13).

The association of hepcidin with the innate immune response comes from the observation of a robust up-regulation of hepcidin gene expression following inflammatory stimuli. In bass, experimental infection with the Gram-positive pathogen, *Streptococcus iniae*, strongly up-regulated hepcidin expression 24 h post-infection (6); and in mouse, hepcidin has been shown to be up-regulated by lipopolysaccharide (7), turpentine (14), Freund's complete adjuvant (15), and adenoviral infections (14). Studies conducted with human primary hepatocytes demonstrated that hepcidin expression responded to addition of IL-6 but not to IL-1α or tumor necrosis factor-α (16). Concordant with this observation, infusion of human volunteers with IL-6 rapidly increased hepcidin production/excretion and was paralleled by a decrease in serum iron and transferrin saturation (17). A strong correlation between hepcidin expression and anemia of inflammation was also found in patients with chronic and inflammatory diseases, including bacterial, fungal, and viral infections (16). These findings, further corroborated in a mouse model, led to the conclusion that induction of hepcidin during inflammation depends on IL-6 and that the hepcidin-IL-6 axis is responsible for the hypoferremic response and subsequent restriction of iron from blood-borne pathogens (17).

Evidence for the essential role of hepcidin in iron homeostasis and hypoferremia of inflammation has come primarily from genetic studies in human and mouse because only two native hepcidin peptides have been purified to date, one from human and the other from bass (1, 2, 6). The structure of human hepcidin shows it to be an amphipathic molecule composed of two distorted antiparallel β-sheets separated by a hairpin loop, containing a vicinal disulfide bond (disulfide bond between adjacent cysteines), and stabilized by three inter-β-sheet disulfide bonds (4). To shed light onto the evolutionary conservation of hepcidin, and its function(s) in innate immunity in bass, we have chemically synthesized and refolded bass hepcidin, and we determined its solution structure and its antibacterial and antifungal activities against a panel of selected human and fish pathogens. We also examined the concept that bass hepcidin acts synergistically with moronecidin, a constitutively expressed antimicrobial peptide, to enhance bass innate immunity. Finally, we examined the temporal aspects of hepcidin gene expression following controlled infections of bass with both Gram-negative and Gram-positive fish pathogens.

EXPERIMENTAL PROCEDURES

Synthesis, Refolding, and Purification of Bass Hepcidin—The Fmoc-amino acid derivatives were obtained from Bachem AG (4416 Bubendorf, Switzerland) and included the following side chain protected derivatives: Arg (2,2,5,7,8-pentamethylchroman-6-sulfonyl), Asn (triphenylmethyl), and Cys (triphenylmethyl). Stepwise assembly was carried out on a Labortec SP6000 peptide synthesizer at the 5-mmol scale starting with Fmoc-Phe-resin. Each coupling was monitored for completeness by using the ninhydrin procedure described by Kaiser *et al.* (18). All couplings were mediated by dicyclohexylcarbodiimide in the presence of 2 eq of 1-hydroxybenzotriazole. Following final removal of the Fmoc group from the peptide resin, 1.0 g of resin-bound peptide was cleaved from the solid support and simultaneously deprotected by using reagent K (19) for 2 h at room temperature. Following cleavage, the peptide was filtered to remove the spent resin beads and precipitated with ice-cold diethyl ether. The crude peptide was collected on a fine filter funnel and washed with ice-cold diethyl ether, yielding 285 mg of crude linear peptide. The crude peptide was subsequently dissolved with 50% (v/v) AcOH in H_2O. The crude, solubilized peptide was subsequently diluted into 1.6 liters of an aqueous buffer containing 2 M guanidinium HCl, 10% isopropyl alcohol, and 10% dimethyl sulfoxide (Me_2SO). The pH of the peptide solution was adjusted to 5.8 with NH_4OH and allowed to undergo oxidative folding at room temperature for 18 h. Following oxidation of the disulfide bonds, the peptide solution was acidified to pH 2.5 and pumped onto a Vydac C_{18} column (2.5 $\times$ 30 cm). The sample was eluted at a flow rate of 8 ml min^{-1} with a stepwise gradient from 10, 20, and 40% acetonitrile into H_2O containing 0.1% trifluoroacetic acid to concentrate the sample. Each of the fractions was analyzed by MALDI and RP-HPLC. The 40% fraction containing the refolded hepcidin was lyophilized resulting in 135 mg of ~40% pure peptide. This fraction was further purified using the same semi-preparative RP-HPLC column and flow rate and a gradient of 10–45% MeCN into 0.1% trifluoroacetic acid in H_2O over 120 min. The resulting fractions were analyzed using two analytical RP-HPLC systems, trifluoroacetic acid and triethylammonium phosphate (20). Pure fractions were pooled and lyophilized. Upon lyophilization, 8.2 mg of bass hepcidin was obtained, representing a yield of 2.9%.

Amino Acid and MALDI-TOF Mass Spectral Analysis—Synthetic peptide samples were hydrolyzed in 6 N HCl at 110 °C for 22 h *in vacuo*. Amino acid analysis was performed on a Beckman 126AA System Gold amino acid analyzer. MALDI-TOF MS analysis was performed on a Kratos MALDI-TOF mass spectrometer using α-cyano-4-hydroxycinnamic acid as a matrix.

Sample Preparation and NMR Spectroscopy—NMR samples were prepared by dissolving ~4 mg of the peptide in 500 μl of H_2O containing 5% ^2H_2O and 0.03% NaN_3 to give a peptide concentration of ~3.5 mM. The unadjusted pH was 4.7, but in some experiments it was adjusted to 4.5 by the addition of CD_3COONa. The pH was measured at 295 K without correction for isotope effects. Spectra were recorded at 278, 298, and 308 K on Bruker Avance 500 (with cryoprobe) and DRX-600 spectrometers. Solvent suppression was accomplished by use of presaturation or the WATERGATE gradient echo sequence (21). Conventional two-dimensional TOCSY, NOESY, DQF-COSY, and E-COSY spectra were obtained using 2048 complex data points in the directly detected dimension and typically 300–400 t_1 increments. A TOCSY spin-lock time of 60 ms and NOESY mixing times of 60 and 250 ms were used. In addition, two-dimensional ^{15}N- and ^{13}C-HSQC experiments were performed at natural abundance isotope levels in order to obtain ^{15}N and ^{13}C resonance assignments, respectively. In these experiments 64 and 256 increments, respectively, were acquired in the indirect dimension and 2048 points in the direct dimension, and decoupling was performed during acquisition. A three-dimensional ^{13}C-HSQC-NOESY experiment was performed at natural abundance in order to resolve peak overlap in the ^1H dimension. Spectra were processed using XWINNMR (Bruker AG) or NMR-pipe (22) with 60° phase-shifted, sine-squared window functions applied in both dimensions and were analyzed using XEASY (version 1.3.13) (23) or nmrDraw (22). Spectra were referenced to the H_2O signal at 4.77 ppm (298 K) or a small impurity at 0.15 ppm. The $^3J_{HNH\alpha}$ coupling constants were measured from DQF-COSY spectra as described previously (24). C^α, C^β, H^α, HN, and N chemical shifts were used in the program TALOS (25) to obtain backbone torsion angle predictions. Sequence-specific resonance assignments were made using standard procedures. The chemical shifts of bass hepcidin have been deposited with BioMagRes-Bank accession number 6085 (www.bmrb.wisc.edu). Diffusion data were obtained using a PFG longitudinal eddy-current delay pulse sequence (26) and incrementing (in 12 points) the amplitude of the field gradient, as described previously (27). To process the data, at least 10 peptide resonances were examined, and the decay of the peak intensities as a function of the field gradient was analyzed and evaluated using XWINNMR.

To identify amide protons potentially involved in hydrogen bonds, the peptide was freeze-dried and resuspended in 500 μl of ^2H_2O at pH 4.5. The disappearance of amide resonances was monitored over the next 12 h with a series of one-dimensional and two-dimensional TOCSY experiments. Slowly exchanging amides were designated as such if they were still observable after 6 h at 298 K. The backbone amide chemical shift temperature coefficients were estimated from spectra acquired at three different temperatures; coefficients of magnitude <4 ppb/K may indicate that the amide is not in free exchange with solvent.

Structural Constraints and Structure Calculations—Cross-peak volumes measured from a 250-ms NOESY spectrum recorded at 600 MHz were used to derive upper bound, inter-proton distance restraints. Conversion from NOE volumes to distance bounds was accomplished using the program CYANA (28). Five predefined classes were employed in CYANA as follows: 1) intraresidue cross-peaks except those between backbone or β-protons; 2) intraresidue and sequential cross-peaks between backbone protons or between backbone and β-protons; 3) medium range (less than five residues apart) cross-peaks between backbone protons or between backbone and β-protons; 4) other (*i.e.* long range) cross-peaks between backbone protons; and 5) all others. The NOESY cross-peak volumes were considered to be proportional to r^{-6} for classes 2–4 and to r^{-4} for classes 1 and 5. All NOE restraints discarded by

CYANA because of peak overlap were included in the weakest class (<5.5 Å). Backbone dihedral angle (ϕ and ψ) constraints were inferred from $^3J_{HNH\alpha}$ coupling constants as described previously (24) or as obtained from TALOS.

CYANA was used for the initial evaluation of upper bound distance restraints. Final structures were generated in X-PLOR-NIH starting from a randomly generated template structure with or without the presence of disulfide bonds and different randomized initial velocity distributions and were subjected to a standard simulated annealing protocol. Fifty structures with the lowest energy were selected from the 100 calculated initially and subjected to further refinement in a water box (29). The best 20 structures based on their stereochemical energies (*i.e.* the sum of all contributions to the calculated energy excluding the electrostatic term) and NOE energies were chosen for structural analysis. Structural analyses were carried out using the programs MOLMOL (30) and PROCHECK-NMR (31). All structural figures were prepared using MOLMOL. The structure of bass hepcidin has been deposited in the Protein Data Bank with accession number 1S6W (32).

Microbial Isolates—*Aeromonas hydrophila*, *Aeromonas salmonicida*, *Edwardsiella tarda*, *Plesiomonas shigelloides*, and *S. iniae* were laboratory isolates recovered from moribund HSB (Kent SeaTech Corp.). Biochemical analysis and ribosomal DNA (16 S) sequencing were used to confirm their identification. All other bacterial isolates were obtained from the American Type Culture Collection (ATCC, Manassas, VA) with the exception of the fungal strain, *Aspergillus niger*, which was provided by Dr. Richard Gallo (Veterans Hospital, San Diego). Logarithmic phase cultures were used in all experiments. Most bacteria and yeast were grown in Luria-Bertani broth (Difco), although streptococcal isolates were grown in Todd Hewitt Broth (THB, Difco). Filamentous fungi were grown in half-strength potato dextrose broth (PDB, Difco) supplemented with tetracycline (10 μg/ml).

Antimicrobial Assays—Minimal inhibitory concentration (MIC) for liquid growth inhibition assay and minimal bactericidal concentration (MBC) were determined as described previously (5, 33). Briefly, bacteria, yeast, and filamentous fungi were incubated in the appropriate growth media in the presence of 2-fold serial dilutions of synthetic bass hepcidin (44–5.5 μM final concentrations). Bacterial growth was measured (A_{600}) after 18 h of incubation at 37 °C. MIC was expressed as the lowest concentration of peptide tested that inhibited microbial growth completely (34). For determination of MBC, bacteria were incubated in 96-well plates in the presence of varying concentrations of hepcidin for 18 h at 37 °C, and aliquots of the cultures were then plated on Todd Hewitt agar, and bacterial growth was assessed after overnight incubation at 37 °C. To examine the rate of bacterial killing of bass hepcidin, kinetic studies were performed using the Gram-negative pathogen *Yersinia enterocolitica*. Briefly, synthetic bass hepcidin (22 and 44 μM) or moronecidin (10 μM) (5) was added to a log phase culture of *Y. enterocolitica* (2×10^5 CFU ml^{-1}) and incubated at 37 °C. Bacterial viability was assessed at 0, 0.5, and 1–3 h by plating serial dilutions of the bacterial suspension on Todd Hewitt agar. CFU counts were performed after overnight incubation at 37 °C. The growth index was calculated as bacterial CFU recovered/CFU at time 0.

Antimicrobial Synergism Studies—Synergism between synthetic bass hepcidin and moronecidin was tested in checkerboard liquid growth inhibition assays. In brief, 2-fold serial dilutions of each peptide were made in water, and 10 μl of the solution was added to the bottom of the wells of a 96-well plate (Costar). Ninety μl of exponential phase bacterial cultures (A_{600} ~0.2) were freshly diluted in culture media to ~2×10^5 CFU ml^{-1} and added to peptide solutions. Controls consisted of wells with the appropriate volume and concentration of each peptide alone or of water. Bacterial viability was assayed at 2 h by plating aliquots of the bacterial suspension for CFU enumeration. The bacterial suspensions were further incubated overnight at 37 °C, and bacterial growth was monitored by absorbance at 600 nm for determination of MIC. Synergistic activity was quantify as fractional inhibition concentration (FIC) index = ([A]/MIC_A) + ([B]/MIC_B), where MIC_A and MIC_B are the MICs of the peptides alone and [A] and [B] are the MICs of A and B when used together (35).

Germination and Fungicidal Assay—Spores of *A. niger* were harvested as described previously (36), resuspended in sterile water containing 0.05% Tween 80, and the concentration adjusted to ~10^8 spores per ml. Spores were diluted in half-strength PDB containing 16 μM chloramphenicol to a final concentration of 10^5 spores per ml. Ninety μl of the suspension was placed in sterile flat-bottomed polystyrene 96-well plates (Costar) with 10 μl of serial dilutions of peptide (440, 220, 110, and 55 μM) in water. Germination of spores was allowed to proceed for 2 days at 30 °C in the dark, after which hyphae density was measured by absorbance at 600 nm. After 2 days of incubation, the contents of wells showing no germination were centrifuged for 3 min at 5000 rpm and resuspended in 50 μl of fresh PDB media, and triplicate aliquots were spotted onto PDB agar plates. Plates were placed at 30 °C for 3 days to monitor germination of hyphae. The absence of germination indicated fungicidal activity.

Hemolytic Activity—Freshly packed striped bass erythrocytes (3 ml) isolated from young fingerlings (~30 g) and adult fish (~300 g) were washed with phosphate-buffered saline (PBS; pH 7.4) until the supernatant was colorless and resuspended in PBS (30 ml) supplemented with glucose (0.2%, w/v). Synthetic bass hepcidin (10 μl of 880–55 μM) was added to 90 μl of a 1% suspension of washed erythrocytes in microcentrifuge tubes. Triplicate samples were incubated for 30, 90, 180, and 240 min at 37 °C and then centrifuged for 10 min at 3500 rpm. Supernatant from the erythrocyte suspension (70 μl) was placed in a microtiter plate, and absorbance at 405 nm was determined. The percentage of hemolysis in hepcidin-treated erythrocytes was expressed relative to hemolysis obtained with a control erythrocyte suspension treated with 0.1% SDS (100% hemolysis).

Bacterial Challenges, Tissue Collection, and RNA Extraction—Thirty HSB fingerlings (43.35 ± 17.51 g) were injected intraperitoneally (IP) with *S. iniae* (3.5×10^5 CFU) or *A. salmonicida* (2.0×10^5 CFU). Fish injected with sterile PBS served as controls. Following challenge, the three groups of fish were maintained in separate 60-liter flow-through tanks receiving aerated water at 25 ± 0.1 °C. For mRNA expression analysis, two individual fingerlings from each challenged group (*S. iniae* and *A. salmonicida*) were selected randomly at five time points post-challenge (4, 8, 16, 24, and 48 h) and anesthetized with MS-222 (Finquel; Argent). Liver tissue (~300 mg) was dissected aseptically and preserved in RNALater (Ambion). Liver samples were also collected from the control group (*i.e.* PBS) pre-challenge (0 h) and at two time points (8 and 24 h) post-challenge. The remaining fingerlings in each group were monitored daily for morbidity and mortality; tissues (brain, head, and kidney) from moribund animals were cultured on tryptic soy agar plates containing 5% sheep blood to confirm the presence of *S. iniae* or *A. salmonicida*. Preserved liver tissues (50 mg) were homogenized in Tri-Reagent (Molecular Research Center), and total RNA was extracted according to the manufacturer's protocol. An additional DNase treatment (RNeasy™ Spin Columns, Qiagen) was performed to further remove any genomic DNA contamination. RNA concentrations were determined spectrophotometrically (A_{260}), and 50 ng μl^{-1} working aliquots were diluted in RNase-free H_2O and stored at −80 °C.

Measurement of Hepcidin Gene Expression—Hepcidin gene expression in infected and mock-challenged HSB fingerlings was quantified using a competitive RT-PCR assay. A homologous RNA competitor (designated as "cHEP") was constructed by using a segment of the bass hepcidin prodomain containing a 50-bp deletion spanning two RT-PCR primer binding sites slightly modified from our earlier study (6), 1403F2 (5′-GAGATGCCAGTGGAATCGTGGAAG-3′) and 86R2 (5′-GAGGCTGGAGCAGGAATCCTCAG-3′). The amplicon resulting from RT-PCR of the competitor hepcidin mRNA (cHEP, 99 bp) was designed to be easily discernible from the native bass hepcidin mRNA ("bHEP," 153 bp) using agarose gel electrophoresis. To generate the competitor, equimolar concentrations (37) of two oligonucleotide primers (cHEP1, 5′-GGATCCGAGATGCCAGTGGAATCGTGGAAGTTGCTGCATTGCTGTCCTAATATGAGCGGATGTGGTGTCTGCTGC-3′; and cHEP2, 5′-GGATCCGAGGCTGGAGCAGGAATCCTCAGAACCTGCAGCAGACACCACATCCGCTCATATTAGG-3′) were annealed using standard conditions, yielding a 109-bp product with 30 bp of complementary overlap, and the product was amplified (FailSafe PCR™; Epicenter) with the primer pair 1403F2 and 86R2. Purified PCR product (PCR Purification Column, Qiagen) was cloned into pCC1, which contained an upstream T7 RNA polymerase promoter, following the manufacturer's instructions (CopyControl™ pCC1 PCR cloning kit; Epicenter). Approximately 100 ng of plasmid vector, containing the modified hepcidin prodomain segment, was linearized with HindIII (Invitrogen) downstream of the insertion site, and *in vitro* transcription was performed using a T7 RNA polymerase (DuraScribe™ T7 transcription kit; Epicenter). Competitor RNA was purified, treated with DNase, and resuspended in RNase-free water following the manufacturer's instructions (RNeasy™ purification kit; Qiagen). RNA concentrations were measured, and aliquots of 10-fold serial dilutions were made (10–0.0001 ng/μl) and stored at −80 °C.

Quantification of Bass Hepcidin Gene Expression—To assess levels of native bass hepcidin mRNA using competitive RT-PCR, total RNA from each liver sample (infected or mock-challenged HSB) was assayed in a series of six single-tube RT-PCRs run in parallel. Each single-tube RT-PCR contained 100 ng of total RNA extracted from the liver, and one of six increasing amounts of hepcidin competitor (0.0001 to 10 ng). A

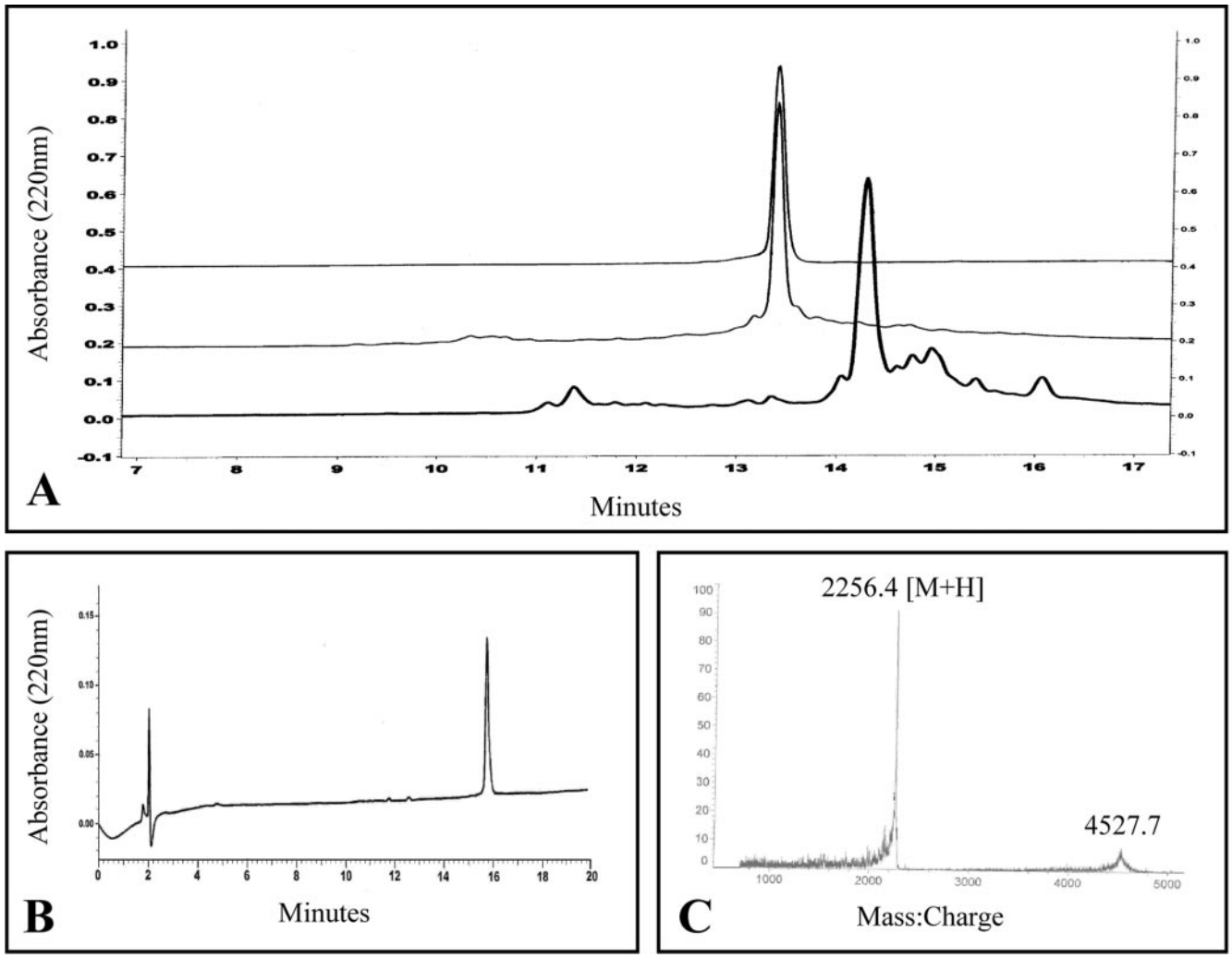

FIG. 1. *A* shows the RP-HPLC oxidation profile from the crude reduced product (*bottom chromatogram*) to the tetradisulfide-linked peptide (*middle chromatogram*) following an 18-h oxidation in 10% Me_2SO. The *top chromatogram* shows the purified product obtained following preparative RP-HPLC. Gradient conditions were 5% MeCN in water containing 0.1% trifluoroacetic acid to 40% MeCN in water containing 0.1% trifluoroacetic acid. *B*, co-elution of a 1:1 mixture of synthetic bass hepcidin with natural material. *C,* MALDI-TOF mass spectrum of the synthetic bass hepcidin.

second, non-competitive RT-PCR was performed to confirm the quality of the RNA samples using PCR primers that amplify a region of 18 S rRNA of HSB (SB18S, SB18Srev). In all cases, RNA was reverse-transcribed and amplified in a single reaction (MasterAmp™; Epicenter) with the primers 1403F2/86R2 or SB18for/SB18rev using the following cycling profile: 1) reverse transcription for 20 min at 60 °C; 2) denaturation for 30 s at 94 °C; 3) annealing for 30 s at 58 °C; 4) extension for 30 s at 72 °C; 5) steps 2–4 were repeated for a total of 20 cycles; and 6) final extension for 2 min at 72 °C. Amplified products were electrophoresed on 2.0% agarose gel stained with ethidium bromide (0.05 $\mu g\ ml^{-1}$). For competitive RT-PCR assays, gel images were digitized using an EDAS 120 electrophoresis documentation system (Eastman Kodak), and mean fluorescent intensities of the PCR products (cHEP and bHEP) were calculated densitometrically using NIH Image 1.63 (www.rsb.info.nih.gov/nih-image). Regression curves were generated from each series of six single-tube RT-PCRs by plotting, on double logarithmic scale, the value of the known competitor quantity (0.0001–10 ng) against the fluorescent signal ratio of the resulting RT-PCR amplicons (cHEP:bHEP). The quantity of native hepcidin mRNA for each sample was determined based on the point of signal equivalence (competitor:target = 1) (38).

RESULTS

Synthesis—Synthesis of bass hepcidin was initiated on Fmoc-Phe-Wang resin using a semi-automated protocol where each coupling was monitored using a colorimetric test to ensure the completeness of the reaction and ultimately superior quality of the crude product. Native bass hepcidin possesses 8 cysteines that form 4 disulfide bridges (6). Therefore, after trifluoroacetic acid deprotection and cleavage, the synthetic peptide was allow to refold and the thiol groups to oxidize under slightly acidic conditions in the presence of organic co-solvents and chaotropic agents to keep the peptide from aggregating and precipitating. Me_2SO was used as an oxidation accelerator according to the method reported by Tam *et al.* (39). Aliquots of the reaction were sampled during oxidation and analyzed by RP-HPLC until the HPLC profiles remained unchanged (after 18 h). The purified synthetic product was determined to be homogeneous by analytical RP-HPLC in two different solvent systems (trifluoroacetic acid and triethylammonium phosphate) and co-eluted with a sample of the native hepcidin form (Fig. 1). Amino acid analysis of purified synthetic bass hepcidin showed the following average amino acid ratios: Asx (2) 2.05; Ser (1) 1.00; Pro (1) 0.97; Gly (3) 3.00; Met (1) 0.31, 0.99; Phe (2) 2.18; Val (1) 0.78; Arg (2) 1.82; and Cys (8) 5.46 (both Cys and Met are partially destroyed during the acid hydrolysis method used). MALDI-TOF mass spectral analysis of the purified synthetic bass hepcidin determined a (M + H) of 2256.4 that was consistent with the molecular mass of the native peptide (2255.97 MH^+). In addition, the synthetic and native bass hepcidin gave the same dose-response killing curve against *E. coli* (data not shown). These observations led us to

conclude that the two molecules are identical. Most interestingly, the MALDI-TOF mass profile showed the presence of a non-covalent dimer as a sodium adduct. This species is consistent with observations in other defensin-like peptides that are known to self-associate and form aggregates.

Initial NMR Spectral Analysis—TOCSY and NOESY experiments acquired at different temperatures showed that, at 278 K, there were a number of unusually broad amide resonances (supplemental Fig. S1). This broadening was reduced at higher temperatures, allowing essentially complete ^{1}H resonance assignments to be made from analyses of DQF-COSY, TOCSY, and NOESY spectra at 298 and 308 K. In addition, the majority of ^{13}C resonances and several backbone amide ^{15}N assignments were assigned from two-dimensional ^{13}C and ^{15}N HSQC spectra, respectively, recorded at natural abundance isotope levels (supplemental Table S1). As noted previously for human hepcidin (4), certain resonances of the 4th and 5th cysteine residues were severely broadened at all temperatures, particularly the NH resonances. The amide resonance of the 5th cysteine was not observed in TOCSY or NOESY experiments at any temperature, and only very weak NH-H^{α} cross-peaks in DQF-COSY spectra enabled this assignment. Amide resonances from Cys^{2}, Arg^{20}, and Phe^{21}, the residues closest to the termini of the peptide, were also broadened at all temperatures. The single proline residue was shown to exist in the *trans* conformation, and there was no evidence of *cis-trans* isomerization. Diffusion measurements at 278 and 298 K gave values of 1.4×10^{-10} and 2.9×10^{-10} m^2 s^{-1}, respectively. Allowing for the difference in water viscosity at these temperatures, these data indicate that the peptide has a similar hydrodynamic radius at both temperatures, thus ruling out temperature-dependent aggregation as the source of line broadening. Amide, H^{α}, and C^{α} assignments indicated that the majority of residues were in β-sheet conformation (supplemental Fig. S2). The C^{β} chemical shifts for each cysteine indicated they were in an oxidized state, as in the native peptide.

Backbone Amides—The temperature dependence of the amide proton chemical shifts was measured, and an amide exchange experiment was carried out to assess potential hydrogen bonding. On the basis of slow solvent exchange and chemical shift temperature dependence, five amide protons were determined to be involved in hydrogen bonds. Based on initial structure calculations, four of these residues, Arg^{3}, Cys^{5}, Gly^{16}, and Cys^{18}, appeared very likely to be involved in two pairs of backbone hydrogen bonds. The first pair was between the amide of Arg^{3} and carbonyl of Cys^{18} and the amide of Cys^{18} and carbonyl of Arg^{3}. The second pair involved the corresponding groups of Cys^{5} and Gly^{16}. The amide protons of these residues had not fully exchanged with solvent deuterium after 12 h at 298 K and also exhibited temperature coefficients $\leq$4 ppb/K. The amide proton of Met^{12} also showed slow exchange with solvent deuterium and a low temperature coefficient. On the basis of initial structure calculations, it seemed likely that the amide of Met^{12} was hydrogen-bonded to the carbonyl moiety of Cys^{9}, a common arrangement in β-type turns; but as this was slightly ambiguous, it was not included in final structure calculations.

Disulfide Bonding Pattern—Mass spectroscopy data on native bass hepcidin had shown previously (5) that all eight cysteines were engaged in disulfide bonds. The synthetic peptide used in this study was shown to be active in a set of antimicrobial assays and was chromatographically equivalent to the native peptide, and thus may be expected to adopt the same structure. A previous study on human hepcidin (4) had determined the disulfide bond linkages for the peptide, including a rare vicinal disulfide bond between the 4th and 5th cysteines, corresponding to Cys^{8} and Cys^{9} in bass hepcidin. To determine whether the same pairings existed in bass hepcidin, the NMR data and structures generated in this study were examined carefully. Because of spectral overlap involving the NH and H^{α} resonances of Cys^{6}, Cys^{8}, and Cys^{19}, severe broadening of the NH resonances of Cys^{8} and Cys^{9}, and overlap of the majority of the Cys H^{β} resonances, the disulfide bonding pattern of bass hepcidin was not obvious from the NMR data alone. Moreover, several Cys resonances showed NOEs to resonances from more than one other Cys residue. Nonetheless, our data imply that bass hepcidin contains the same disulfide-bonding pattern as found in human hepcidin based on the following observations. An examination of the NOEs observed for each cysteine (supplemental Fig. S3) shows that Cys^{6} and Cys^{15} have NOEs only to each other and not to any other cysteines, implying that they are disulfide-linked. Initial structure calculations performed without any disulfide bond constraints showed clearly that Cys^{2} and Cys^{19} also form a disulfide bridge. A number of long range NOEs were observed in support of these linkages, in particular a very strong H^{α}-H^{α} NOE between Cys^{2} and Cys^{19}, as well as weak H^{β}-H^{α} and H^{α}-HN NOEs. The two pairs of hydrogen bonds described above between Arg^{3} and Cys^{18} and Cys^{5} and Gly^{16} are fully consistent with Cys^{2}–Cys^{19} and Cys^{5}–Cys^{18} disulfide links. Strong H^{α}-H^{α} and H^{α}-HN NOEs were also observed between Cys^{6} and Cys^{15}.

Of the three possible disulfide pairings between the other four cysteines (Cys^{5}, Cys^{8}, Cys^{9}, and Cys^{18}), only one (Cys^{5}–Cys^{9} and Cys^{8}–Cys^{18}) was not supported by NOE data or structure calculations. All potential hydrogen bonds identified by amide exchange experiments were equally well satisfied by both structures. These two possibilities could not be resolved on the basis of the presence of particular NOEs. The Cys^{5}–Cys^{8} and Cys^{9}–Cys^{18} pairing, however, would bring several protons from Cys^{8} and Cys^{9} into close proximity (<3.5 Å) to protons from Cys^{18}. No NOEs were observed between residues 8 or 9 and 18, although overlap and the broadening of the Cys^{8} and Cys^{9} amides could, in part, explain this observation. Further support for a vicinal disulfide link comes from the severe broadening of the amide resonances of both Cys^{8} and Cys^{9} compared with all other residues except those at the termini. As all adjacent and nearby residues display sharp linewidths, whatever is causing the broadening is localized to Cys^{8} and Cys^{9}. The formation of a vicinal disulfide bond would create a closed eight-atom loop that may be conformationally mobile. If the mobility of the loop were on an intermediate (NMR) time scale, this would lead to line broadening for those resonances.

Analysis of structure calculations performed with the two possible disulfide connectivities showed that NMR-derived distance and angular restraints were better satisfied by the Cys^{5}–Cys^{18} and Cys^{8}–Cys^{9} pairings, although NOE violations for the other possible pairing were all <0.3 Å. In contrast, the *overall* energy of the vicinal disulfide-containing structure was slightly higher than the alternative, as the formation of a vicinal disulfide leads to a slightly non-planar peptide bond between the two cysteines ($\Omega = 175^{0}$), as well as unfavorable χ^{1} angles (χ^{1} = 86° and −31° for Cys^{8} and Cys^{9}, respectively) (40). Structure calculations run with no disulfide bond restraints gave an identical structure to calculations performed with the same disulfide pattern as human hepcidin (the backbone r.m.s.d. between the closest-to-average structure of each family over residues 2–19 was 0.56 Å), but not to calculations performed using a starting structure containing the other potential disulfide connectivities (corresponding backbone r.m.s.d. 1.51 Å; Fig. 2). Taken together, these data provide strong evidence that bass hepcidin shares the same disulfide bonding pattern as human hepcidin.

Solution Structure—Parameters and structural statistics

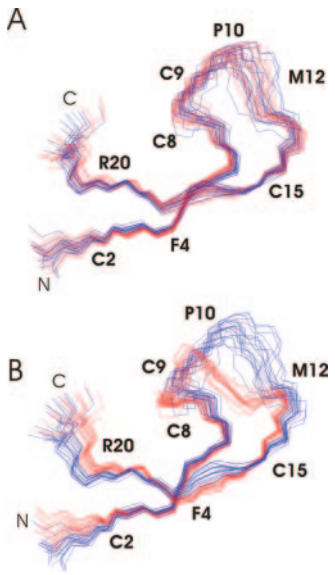

FIG. 2. **Structures calculated with different disulfide bonding patterns.** Structures calculated with a 2–19, 5–18, 6–15, and 8–9 (vicinal) disulfide bonding pattern (*A*) and 2–19, 5–8, 6–15 and 9–18 disulfide bonding pattern (*B*) are shown in *red*, compared with structures generated without any disulfide restraints (*blue*). The structures generated using the vicinal disulfide bond containing pattern show a much greater similarity to those generated in the absence of any disulfide restraints and show a greater conformity to observed NOEs. This figure was prepared using MOLMOL (30).

TABLE I
Summary of experimental restraints and structural statistics for bass hepcidin

No. distance restraints	188
Intraresidue ($i = j$)	38
Sequential ($\|i - j\| = 1$)	65
Medium range ($1 < \|i - j\| < 5$)	17
Long range ($\|i - j\| > 5$)	64
Hydrogen bonds	4
No. dihedral restraints	23
Energies	
E_{NOE} (kcal mol^{-1})[a]	1.19 ± 0.42
Deviations from ideal geometry[b]	
Bonds (Å)	0.0050 ± 0.0002
Angles (°)	0.646 ± 0.011
Impropers (°)	0.594 ± 0.024
r.m.s.d. (Å)[c]	
Backbone heavy atoms (2–19)	0.80 ± 0.25 Å
Backbone heavy atoms (2–7, 13–19)	0.61 ± 0.23 Å
All heavy atoms (2–19)	1.32 ± 0.26 Å
All heavy atoms (2–7, 13–19)	1.20 ± 0.25 Å
Ramachandran plot[d]	
Most favored (%)	65.9
Additionally allowed (%)	28.4
Generously allowed (%)	5.6
Disallowed (%)	0.0

[a] The value for NOE energy was calculated from a square well potential with force constants of 50 kcal mol^{-1} Å^2.
[b] The values for the bonds, angles, and impropers show the deviations from ideal values based on perfect stereochemistry.
[c] r.m.s.d. over the backbone heavy atoms (N, C$^\alpha$, C') of all residues.
[d] As determined by the program PROCHECK-NMR for all residues except Gly and Pro (31).

characterizing the final 20 structures of bass hepcidin are summarized in Table I, and stereo views of the structures superimposed over the backbone are shown in Fig. 3. Angular order parameters showed that, apart from the N-terminal glycine, the backbone dihedral angles ϕ and ψ were all well ordered, as were the majority of the side chain χ^1 angles (supplemental Fig. S4). The peptide forms a two-stranded, slightly distorted, antiparallel β-sheet with a flexible hairpin loop from Asn^7 to Gly^{14} that lies above the concave surface of the sheet. Bass hepcidin is well structured over the majority of its length (residues 2–19). The degree of curl of the loop region could not be defined precisely with the available restraints, possibly indicating that it is inherently more flexible than the rest of the molecule. This is supported by the observation that residues 11–13, in the center of the loop, displayed sharp linewidths (supplemental Fig. S1). However, the side chain resonances of Met^{12} showed several NOEs to protons in the β-sheet, reflecting some degree of rigidity. Bass hepcidin is positively charged by virtue of the two Arg residues, and it does not contain any acidic residues. The locations of the Phe and Val side chains from the β-sheet region both lie on the convex surface of the sheet, thus giving the β-sheet a hydrophobic surface, as seen in human hepcidin. Consecutive disulfide bridges lie on alternate sides of the β-sheet (Fig. 3), also seen in human hepcidin. The β-sheet is stabilized by three inter-strand disulfide bonds and four inter-strand hydrogen bonds.

Antimicrobial Spectrum of Activity—Serial dilutions of synthetic hepcidin, beginning at 44 μM, were tested *in vitro* in liquid growth inhibition assays against 21 bacterial strains, a filamentous fungi, and a yeast strain (Table II). The peptide was active against a panel of Gram-negative bacteria including three *E. coli* strains, *P. shigelloides*, *Klebsiella pneumoniae*, *Shigella sonnei*, *Shigella flexneri,* and *Y. enterocolitica*. Hepcidin was not active at 44 μM against another *Klebsiella* sp., *Klebsiella oxytoca*, as well as nine other Gram-negative species tested. The minimum inhibitory concentrations of synthetic hepcidin against Gram-negative bacteria ranged from 5.5 to 44 μM, and overall, 8/18 (44%) of the Gram-negative species tested were sensitive to bass hepcidin. The MBCs were either equal to or twice the MIC for all bass hepcidin-sensitive strains (Table II). Bass hepcidin showed no activity at 44 μM against the three Gram-positive bacteria and single yeast strain tested. Hepcidin displayed antifungal activity *in vitro* against *A. niger* at relatively high concentrations (44 μM; Table II). Most interestingly, hepcidin was not active against any of the key fish pathogens we tested, including the Gram-positive pathogen, *S. iniae*, and the Gram-negative pathogens, *A. hydrophila*, *A. salmonicida*, and *E. tarda*.

Microbicidal Kinetics—An experiment was conducted to examine the microbicidal kinetics of bass hepcidin and to compare its killing activity to another bass antimicrobial peptide, moronecidin. Moronecidin is a 22-amino acid, linear, amphipathic α-helical peptide that was originally co-purified from the gill of HSB with hepcidin (5). These experiments were carried out using *Y. enterocolitica*, where the MIC for hepcidin and moronecidin were measured at 22 and 5 μM, respectively. We compared the killing kinetics of hepcidin and moronecidin against *Y. enterocolitica* at 30-min intervals over a 3-h time period using 2× their MIC concentrations for this organism (44 and 10 μM; Fig. 4). The bactericidal activities of the peptides were assessed by plating cultures and counting CFUs after overnight incubation at 37 °C. Bass moronecidin killed *Y. enterocolitica* within minutes of exposure to the bacteria, leading to a 90% decrease in CFU after 30 min, whereas *Y. enterocolitica* cultures were actually growing in the presence of 22 and 44 μM bass hepcidin at this time. Two and half hours were required for a similar 90% reduction of CFU from the original inoculum with hepcidin at 44 μM. The microbicidal activity of hepcidin was temperature-dependent as was observed for moronecidin (data not shown) (5).

Fungicidal Activity—A germination assay with spores of the filamentous fungi, *A. niger,* was conducted to test the fungistatic and fungicidal activities of the bass hepcidin and to compare them with those of moronecidin (Fig. 5). No hyphae were observed at a peptide concentration of 44 μM after 2 days of incubation at 30 °C. At lower concentrations, the peptide

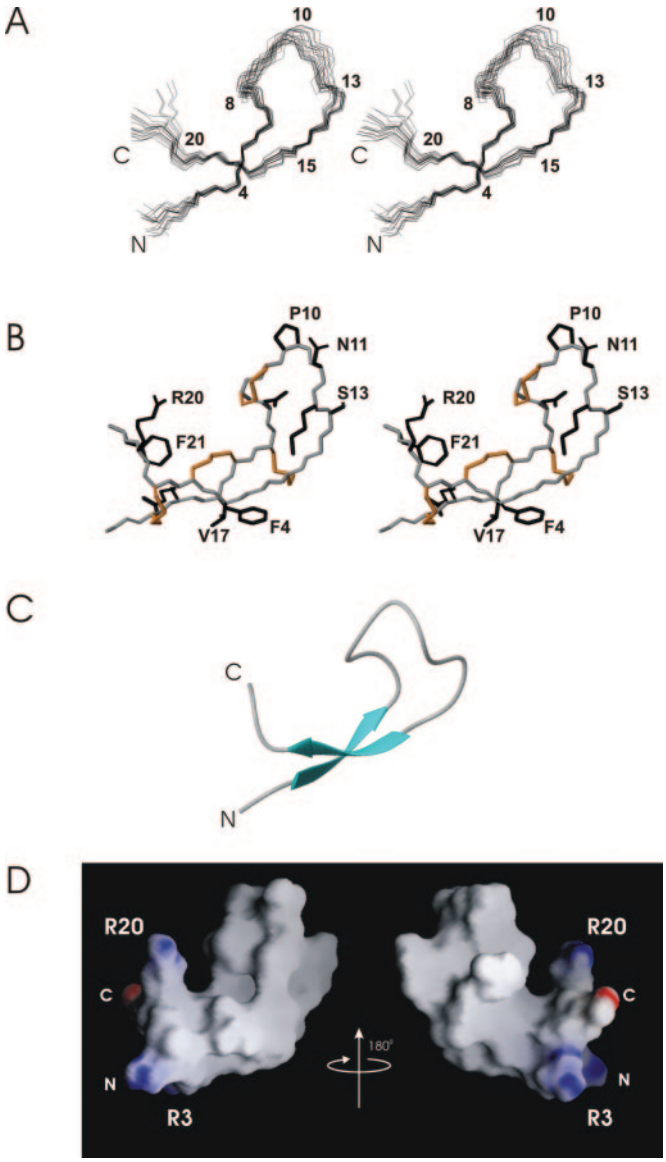

FIG. 3. *A*, stereo view of the backbone atoms of the family of structures generated for bass hepcidin. The two termini are shown, and several of the residues are numbered. *B*, stereo view of a representative structure of bass hepcidin showing the backbone heavy atoms (*gray*), side chain heavy atoms (*black*), and disulfide bonds (*orange*). *C*, ribbon diagram of bass hepcidin showing the antiparallel β-sheet (*blue*) and loop region. *D*, two views of a surface representation of bass hepcidin. The surface is colored with basic residues in *blue* and acidic residues in *red*. The two views are related via a 180° rotation about the vertical axis. *A–C* of this figure were prepared using MOLMOL (30), and *D* was prepared using GRASP (69).

TABLE II
Summary of MIC and MBC of bass hepcidin for various microorganisms

Microorganisms	ATCC no.[a]	MIC	MBC
Gram-positive bacteria			
Entercoccus faecalis (VRE)[b]	51,299	>44	NT[c]
S. aureus (MRSA)[d]	33,591	>44	NT
S. iniae	KST[e]	>44	NT
Gram-negative bacteria			
Aeromonas hydrophilia	KST	>44	NT
A. salmonicida	KST	>44	NT
Enterobacter cloacae	35,030	>44	NT
E. coli	25,922	22	22
E. coli	351,50	22	44
E. coli	D31	11	11
E. tarda	KST	>44	NT
K. oxytoca	49,131	>44	NT
K. pneumoniae	10,031	22	44
P. shigelloides	KST	11	22
P. aeruginosa	35,032	>44	NT
Salmonella arizonae	13,314	>44	NT
Salmonella choleraesuis	14,028	>44	NT
Salmonella typhimurium	13,311	>44	NT
Serratia marcescens	8100	>44	NT
S. flexneri	12,022	22	44
S. sonnei	9290	44	44
Yersinia enterocolitica	23,715	22	22
Filamentous fungi			
A. niger		44	NT
Yeast			
C. albicans	66,027	>44	NT

[a] ATCC indicates American Type Culture Collection number.
[b] VRE, vancomycin-resistant enterococcus.
[c] NT, not tested.
[d] MRSA, methicillin-resistant *S. aureus*.
[e] Kent SeaTech isolates from HSB. The highest concentration tested with bacteria and yeast was 44 μM, and 88 μM was used for the fungi *A. niger*.

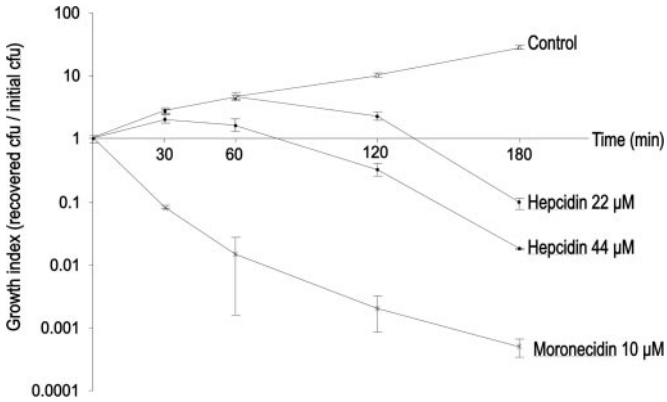

FIG. 4. **Synthetic bass hepcidin at 22 μM (2× MIC or 1× MBC) and 44 μM and synthetic moronecidin at 10 μM (2× MIC and 2× MBC) or water control was added to freshly diluted (1×10^5 CFU ml^{-1} in LB) logarithmic phase culture of *Y. enterocolitica* and incubated at 37 °C.** Aliquots of the culture were removed at various time points, diluted in PBS, and plated on THB for colony count. Growth index was calculated as bacterial CFU recovered/initial inoculum. Each point represents an average of three experiments, and the *vertical bars* show the S.D.

caused delayed growth of hyphae with abnormal morphology (data not shown). After 48 h of exposure to the respective peptides, spores were removed and cultured in fresh medium and examined 48 h later for growth. Bass hepcidin was fungistatic at low concentrations with a lower IC_{50} concentration (peptide concentration giving 50% growth inhibition) than moronecidin (5 *versus* 7 μM) when tested in parallel assays. Moronecidin, however, was fungicidal at 10 μM, whereas hepcidin was fungicidal at 44 μM (Fig. 5).

Synergism between Bass Hepcidin and Moronecidin Antimicrobial Activities—Bass hepcidin and moronecidin were originally co-purified from gill tissues of hybrid striped bass (5, 6), thus opening the possibility that these peptides are co-localized in this tissue and may act additively or synergistically to kill invading microorganisms. To test for synergism between the two antimicrobial peptides *in vitro*, we conducted liquid growth inhibition/killing experiments with a Gram-positive (*S. iniae*) and a Gram-negative bacterium (*Y. enterocolitica*) using varying concentrations of the two synthetic peptides. The bacteria were cultured in the presence of synthetic bass hepcidin and moronecidin and plated after 2 h of incubation at 37 °C for determination of CFU (Fig. 6*A*). We observed (Fig. 6*A*) that 2-fold decreases in the MIC of each peptide for *Y. enterocolitica*, when in combination, reduced CFUs by more than 100-fold below that of either moronecidin or hepcidin alone at their MIC concentrations for this bacteria. A 4-fold decrease in the MIC of

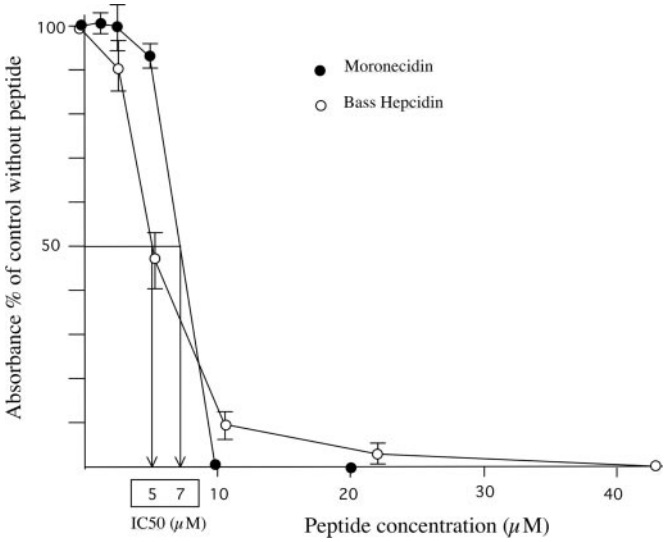

FIG. 5. **Antimicrobial bass hepcidin (○) and moronecidin (●) were added at different concentrations to 10^5 spores ml^{-1} of *A. niger*.** Hyphae density was measured at 600 nm after 48 h at 30 °C and represented as a percentage of absorbance with 100% corresponding to hyphae density without peptide. The IC_{50} values represent the peptide concentration giving 50% growth inhibition. Results show average of three experiments, and *vertical bars* show S.D.

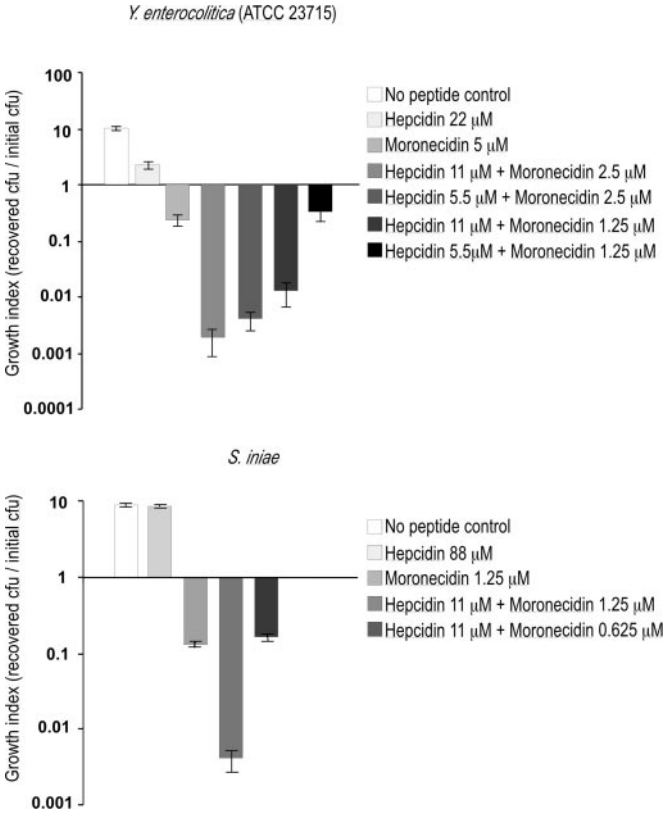

FIG. 6. **Exponential phase cultures of *Y. enterolitica* or *S. iniae* diluted in THB to 10^5 CFU ml^{-1} were incubated for 2 h with the indicated concentrations of hepcidin, moronecidin, or water as a control.** Aliquots of the bacterial suspensions were plated for enumeration of CFU after overnight incubation. The growth index was calculated as bacterial CFU recovered/CFU before addition of the peptide. The experiment was performed in triplicate for each sample. *Vertical bars* represent S.D.

each peptide in combination yielded similar or better killing of *Y. enterocolitica* than either peptide alone at their MIC (Fig. 6 *A*). Bass hepcidin had no detectable antimicrobial activity against *S. iniae* after 2 h of incubation with concentrations as high as 88 μM (Fig. 6*B*). However, at a hepcidin concentration eight times lower (11 μM), in the presence of 1.25 μM moronecidin, strong killing of *S. iniae* was observed. Under these conditions, a 10-fold reduction in CFU below that of 1.25 μM moronecidin was observed. Although the results shown in Fig. 6, *A* and *B,* give a more intuitive visualization of the synergism between the two peptides, the standard measure for synergism is through calculation of the FIC (41). We calculated FIC indices against a Gram-positive bacteria (*S. iniae*) and three Gram-negative bacteria (*E. coli*, *Y. enterocolitica*, and *S. sonnei*) (Table III). An FIC index of 0.5 indicates strong synergy (representing the equivalent of a 4-fold decrease in the MIC of each compound tested), whereas an FIC index of 1.0 indicates that the antimicrobial activity of the two compounds are additive (*i.e.* a 2-fold decrease in the MIC of each compound tested). The FIC indices calculated for hepcidin and moronecidin were between 0.5 and 0.75, indicating good to moderate antimicrobial synergy between the two peptides.

TABLE III
FIC indices for hepcidin and moronecidin against selected bacteria

Species ([A]/[B])[a]	MIC		Lowest FIC index
	Hepcidin	Moronecidin	Hepcidin + moronecidin
	μM		
S. iniae	>88	2.5	0.56 (11/1.25)
E. coli	22	5	0.75 (5.5/2.5)
Y. enterocolitica	22	5	0.50 (5.5/1.25)
S. sonnei	22/44	5	0.75/0.5 (11/1.25)

[a] FIC index = $[A]/MIC_A + [B]MIC_B$, where MIC_A and MIC_B are the MICs of peptides A and B alone and [A] and [B] are the MICs of peptides A and B in combination. The MICs for the peptides alone are as given in Table II. The numbers in parentheses are the MICs in combination (hepcidin/moronecidin). Since hepcidin MIC against *S. iniae* is higher than 88 μM, the highest concentration we tested, we chose this value as the hepcidin MIC in the calculation of the FIC index.

Hemolytic Activity—The hemolytic activity of bass hepcidin was tested with erythrocytes from HSB. Bass hepcidin displayed essentially no hemolytic activity toward HSB erythrocytes (Table IV). Greater than 98% of the bass erythrocytes exposed to 44 μM hepcidin for 3 h at 37 °C remained intact. This exposure corresponds to a time point when 96% of *Y. enterocolitica* exposed to 44 μM hepcidin have been killed (see Fig. 6*A*). After 4 h of incubation with 44 μM hepcidin, more than 97% of the erythrocytes remained intact. No hemolysis was observed after 4 h at hepcidin concentrations of 11 μM and lower.

Temporal Analysis of Bass Hepcidin Gene Expression Following Bacterial Infection—In a previous study by our group, levels of hepcidin gene expression were assessed at 24 h by kinetic RT-PCR between HSB infected by immersion in a live suspension (5×10^7 CFU ml^{-1}) of the virulent fish pathogen *S. iniae* and mock-challenged controls. Those studies demonstrated that hepatic hepcidin expression in bass was strongly up-regulated (~4,500-fold) following infection with this Gram-positive bacterium (6). However, these experiments only examined a single pathogen and time point post-infection under conditions that did not allow the pathogen dose received by the HSB to be quantified. To extend this study, we examined hepcidin gene expression at intervals over the first 48 h post-challenge following IP injection of a defined dose of *A. salmonicida* or *S. iniae*. HSB fingerlings infected with either *A. salmonicida* or *S. iniae* exhibited 44 and 78% cumulative mortality, respectively, over the course of 7 days. Both pathogens were recovered from the head kidney (*A. salmonicida*) and brain/head kidney (*S. iniae*) of moribund fingerlings, confirming the presence of an active systemic infection. No mortalities occurred in mock-challenged fingerlings, and neither pathogen was recovered from the sacrificed control HSB. Differences in hepcidin expression between experimental HSB fingerlings in-

TABLE IV
Hemolytic activity of bass hepcidin for bass erythrocytes over time

Hepcidin	30 min	90 min	180 min	240 min
μM				
5.5	0	0	0	
11	0	0	0	
22	0	0	0.4 ± 0.15[a]	0.4 ± 0.4
44	0	0	1.4 ± 0.3	2.5 ± 1.2

[a] Hemolytic activity is expressed as percent of controls ± S.D.

fected with either *A. salmonicida* or *S. iniae* were readily apparent using competitive RT-PCR, especially when comparing hepcidin expression between infected and PBS injected control animals at 24 h (Table V; for example of single fish/time point experiment, see supplemental Fig. S5A). Temporal differences in hepcidin expression were also readily apparent following experimental infection with *S. iniae* (supplemental Fig. S5B).

Hepcidin mRNA copy number was low in the livers of healthy control HSB fingerlings at time 0 and at 24 h, comprising $\sim 6 \times 10^{-5}$% of total RNA in liver ($4.37–4.93 \times 10^3$ copies ng^{-1} RNA). Resting levels of hepcidin mRNA in bass liver were ~5–7 fg ng^{-1} total RNA (data not shown). Hepcidin gene expression in bass fingerlings was rapidly up-regulated following IP challenge with *S. iniae* and *A. salmonicida*, Gram-positive and Gram-negative organisms, respectively. For both fish pathogens, hepcidin expression increased roughly 3 orders of magnitude between 4 and 8 h, 4 orders of magnitude by 16 h, and nearly 5 orders of magnitude by 48 h (Table V). Hepcidin hepatic gene expression levels reached >50% and >60% of their 48 h peak levels by 16 and 24 h, respectively, and continued to increase through the end of the experiment at 48 h. Hepcidin mRNA comprised ~3% of the total liver RNA at 48 h post-infection ($2.3–2.4 \times 10^8$ copies ng^{-1} total RNA). The rate of increase and overall levels of bass hepcidin mRNA was strikingly similar in HSB fingerlings challenged with similar inocula of either Gram-negative (*A. salmonicida*; 2.3×10^8 copies ng^{-1} RNA at 48 h) or Gram-positive (*S. iniae*; 2.4×10^8 copies ng^{-1} RNA at 48 h) fish pathogens (Table V).

DISCUSSION

This is the first report characterizing the structure and antimicrobial activities of a non-mammalian hepcidin peptide. Our findings indicate that the bass and human hepcidin peptides adopt a very similar three-dimensional structure and have the same disulfide-bonding pattern. They also both contain a rare vicinal disulfide bond, indicating that key structural attributes for the hepcidin are conserved between human and fish. Our previous work and this study show that many of the defining characteristics of both the genes and the mature peptides are remarkably similar between bass and human.

Structure—The structures of bass and human hepcidin show significant similarity (4). The amino acid sequences of the two molecules share 52% homology and 62% similarity. Both molecules consist of a slightly twisted, two-stranded, antiparallel β-sheet connected by a more flexible hairpin loop that curls over the concave surface of the β-sheet. The β-sheets of the two hepcidins display similar hydrogen bonding patterns and similar close contacts across the sheet. They also share the same disulfide-bridging pattern. The major difference is that the N- and C-terminal arms of bass hepcidin cross over one another to a much greater degree than in human hepcidin. Human hepcidin consists of a hydrophobic surface on the convex face of the molecule and a positively charged concave surface. Whereas bass hepcidin shows a similar hydrophobic convex surface, the clustering of charged residues is most apparent at one end of the molecule. This region contains the N and C termini and the two positively charged Arg guanidino groups, whereas the rest of the molecule is uncharged (Fig. 3*D*). It is interesting to note that bass hepcidin shares many structural characteristics with other antimicrobial peptides (42). Bass hepcidin is as follows: (i) cationic with an overall charge of +1.7 at neutral pH, (ii) adopts an amphipathic structure (42), and (iii) contains a β-hairpin structure cross-linked with disulfide bridges as has been observed in antimicrobial peptides purified from arthropods (tachyplesin, thanatin, and gomesin) (43–45) and mammals (protegrin, θ-defensin-like, and lactoferricin B) (2, 46, 47).

Vicinal Disulfide in Hepcidins—Vicinal disulfides distort the local backbone structure significantly, resulting in an energetically unfavorable non-planar peptide bond as well as unfavorable fixed side chain χ^1 angles. The backbone torsion angles around the vicinal disulfide and the disulfide torsion angles observed in bass hepcidin are in good agreement with those of human hepcidin (4), as well as other proteins containing vicinal disulfide bonds (40, 48, 49). The amide resonances for the two Cys residues forming the vicinal disulfide bond displayed severely broadened line widths, as observed in human hepcidin, but in contrast to all surrounding residues. One explanation for this is that the eight-membered closed loop formed by the cystine could be undergoing conformational exchange on an intermediate NMR time scale. Most interestingly, the amide protons displayed the broadest line widths, whereas the H^{α} and H^{β} protons were not significantly broadened. Such conformational exchange does not indicate that the structure is unstable or reactive but it may be functionally significant. A recent review (40) has highlighted that vicinal disulfide bonds share a number of common stereochemical features, including a non-planar peptide bond in the *trans* conformation, and they are often located in the center of a type VIII β-turn in the peptide backbone. Bass hepcidin also contains a non-planar peptide bond between the cysteines and the ϕ/ψ angles of the two residues (Cys^8 −70/−40°, and Cys^9 −150/156°) are very close to those of a model type VIII turn (residue $(i + 1)$ −60/−30° and residue $(i + 2)$ −120/120°).

The vicinal disulfide bond is known to be functionally significant in a number of different proteins. A spider toxin retains the same fold but loses its neurotoxic activity following reduction of the vicinal disulfide (48). Other proteins such as methanol dehydrogenase (50) and the acetylcholine receptor (51) lose activity upon reduction of their vicinal disulfide bonds. In addition, the vicinal disulfide bond in mercuric ion reductase is believed to be important in mercuric ion binding (52). The different local conformation associated with a reduced or oxidized vicinal disulfide bond has led to speculation that such an entity may form a "redox-activated conformational switch" (40). The vicinal disulfide bond in bass and human hepcidin is located in the loop region of the molecule that is the most flexible part of the structure and shows the highest degree of sequence diversity between species. The combination of flexibility, sequence diversity, and the significance of the vicinal disulfide bond leads us to speculate that the loop region of hepcidin is, functionally, the most important part of the molecule.

Antimicrobial Activities—In this study we examined the spectrum for bass hepcidin of antimicrobial activity against 21 species of bacteria including strains tested previously with human hepcidin. Consistent with studies of human hepcidin, bass hepcidin was active against *E. coli* but had little or no detectable activities against *Pseudomonas aeruginosa*, *Staphylococcus aureus, or Candida albicans* (2). Bass hepcidin and human hepcidin were also both active against *A. niger* in spore germination assays. Our results indicate that bass hepcidin and human hepcidin were both active in a similar range of concentrations against Gram-negative bacteria (2). The anti-

TABLE V
Hepcidin mRNA expression in bass liver following infectious challenge

Hour	Control copy no.[a]	Range	*A. salmonicida* mean copy no.	Range	*S. iniae* mean copy no.	Range
0	4.37×10^3	$1.27–7.46 \times 10^3$	4.37×10^3	$1.27–7.46 \times 10^3$	4.37×10^3	$1.27–7.46 \times 10^3$
4			5.23×10^6	$5.45 \times 10^5–9.92 \times 10^6$	1.06×10^6	$9.78 \times 10^5–1.14 \times 10^6$
8			1.96×10^7	$1.54–2.38 \times 10^7$	1.54×10^7	$3.73 \times 10^6–2.72 \times 10^7$
16			1.17×10^8	$1.02–1.32 \times 10^8$	1.39×10^8	$1.16–1.61 \times 10^8$
24	4.93×10^3	$2.39–7.46 \times 10^3$	1.44×10^8	$8.9 \times 10^7–1.99 \times 10^8$	1.63×10^8	$1.56–1.70 \times 10^8$
48			2.30×10^8	$1.66–2.93 \times 10^8$	2.40×10^8	$1.89–2.92 \times 10^8$

[a] Copy number is average of two HSB individuals expressed in copies ng^{-1} total liver RNA

microbial potency of bass hepcidin contrasted sharply with another bass AMP, moronecidin, that was also purified from HSB gill tissue (5). Moronecidin is a 22-amino acid, linear, cationic peptide with an amphipathic, α-helical structure that exhibits a more potent, broader spectrum of bactericidal activity than hepcidin (5). Peptides like moronecidin are thought to aggregate and interact with negatively charged bacterial membrane components and to disrupt them by forming pores or solubilizing the membrane via a "detergent" effect (53–55). This direct membrane disruption is believed to kill the bacterium by creating osmotic imbalance and loss of cytoplasm. Bass hepcidin is cationic and adopts an amphipathic structure in solution and thus has the potential to interact with and disrupt bacterial membranes like linear, α-helical peptides. Our studies with *Y. enterocolitica* demonstrate that *in vitro* hepcidin kills this bacterium much more slowly than does moronecidin. This may reflect inherent biophysical differences between the two peptides (56). Hepcidin is less cationic and amphipathic than moronecidin. Both of these parameters have been shown to be important structural attributes for potent antimicrobial activity (57). Alternatively, *Y. enterocolitica* is known to have an efflux pump/potassium antiporter to combat the antimicrobial activities of host cationic peptides. Thus, the differences in bactericidal activity between the two peptides may reflect different susceptibilities of the peptides to this antibiotic resistance mechanism (58). Finally, hepcidin may kill bacteria by a mechanism independent of membrane permeabilization (*e.g.* inhibiting a key metabolic process), which may require prolonged contact with the bacteria to exert microbicidal activity. Further investigation is required to elucidate the mode of action for hepcidin.

Hepcidin Expression in Vivo Following Infection—Our results show that infection of bass with either a Gram-positive (*S. iniae*) or Gram-negative (*A. hydrophila*) fish pathogen induces hepcidin gene expression in the liver with very similar kinetics. The first hepcidin transcripts were detected within hours following experimental infections, and expression was maximal at 48 h post-infection. The rapidity and remarkable amplitude of this expression profile are consistent with the acute phase response to infections observed in mammals. Human and mice hepcidin expression both require the inflammatory cytokine IL-6, thus defining hepcidin as a type II acute phase response protein (17). To date, quantitative hepcidin expression in mice has not been quantified following bacterial infections to allow comparison to our fish model. However, mice do show a 4-fold increase in hepcidin expression in response to inflammatory stimulators (14). Other studies in human patients with anemia of inflammation show up to 100-fold greater concentrations of hepcidin in their urine (16).

Despite the limited spectrum and potency of hepcidin antimicrobial activity observed *in vitro*, there are several possible mechanisms by which hepcidin could be effective *in vivo* as an antimicrobial compound (1, 3, 59). It is possible that tissue concentrations of hepcidin reach higher levels than we tested *in vitro*, compensating for the levels of specific activity observed *in vitro*. The dramatic up-regulation of hepcidin expression in liver and other tissues upon experimental infection of HSB with fish pathogens supports this hypothesis (6). In this study, bass liver hepcidin expression increased 3 orders of magnitude within 16 h of infection, 4 orders of magnitude within 24 h, and was nearly 5 orders of magnitude above base line by 48 h post-infection. The magnitude and duration of the up-regulation of hepcidin expression in the liver following infection suggests that high concentrations of hepcidin are important to the innate immune response against these pathogens. Another mechanism by which hepcidin may potentially exert strong antimicrobial effects *in vivo* is through synergistic interactions with other inducible acute phase response proteins and/or constitutively expressed antimicrobial compounds in the tissues. There are a number of examples of co-localization of antimicrobial compounds in various tissues and cell types, as well as specific evidence of synergistic activity when AMPs are combined *in vitro* (60–62). Our previous studies have demonstrated that both the hepcidin and moronecidin genes are expressed in the gill tissue of bass and that their mature peptides reside in this tissue (5, 6, 63). Thus, our demonstration of synergism between hepcidin and moronecidin antimicrobial activities *in vitro* against both Gram-positive and Gram-negative bacteria may reflect an elegant addition to innate immune systems of teleosts. A model where the inducible hepcidin peptide acted synergistically with constitutively expressed AMPs such as moronecidin would predict an increased broad spectrum antimicrobial defense during the early stages of an infection.

Hepcidin, Inflammation, and Hypoferremia—In mammals, hepcidin plays a key role in the hypoferremic response during inflammation, and given the similarity of the two structures and activities, there is potential for a similar role for hepcidin in bass and other teleosts (3, 16, 59). Bacterial pathogens require iron for growth, and most have evolved sophisticated mechanisms for obtaining iron from their hosts to support their proliferation (64). In this regard, hepcidin has been proposed to help combat infection by restricting iron availability to invading pathogens through a strong hypoferremic response, and thus limiting their proliferation (see reviews by Ganz (3) and Ashrafian (65)). The potential for hepcidin-induced hypoferremia in fish is consistent with studies in trout and salmon, where lower free iron in plasma was observed 24–48 h after injection of lipopolysaccharide (66, 67). In addition, symptoms of anemia have been observed in bass infected with *S. iniae* or *A. salmonicida,* both of which we have shown to be potent inducers of hepcidin expression (6, 68).

Strong conservation of the structure and rare vicinal disulfide between bass and human suggests that the hepcidins are functionally constrained from sequence divergence. Because bass hepcidin does not contain any acidic residues, it is not surprising that we found no evidence of direct binding of bass hepcidin to ferric iron by NMR (data not shown). Our data suggest that hepcidin has the potential to exert its effects on the innate immune response of teleosts through a combination

of activities. The bass model employed in these studies should provide a powerful approach to further elucidate hepcidin function(s), including it potential role in hypoferremia in teleosts.

Acknowledgments—We thank Steve Taylor for generous support in the early stages of this project. We thank Yann Lefievre, Daniel Nugent, Ilya Khaytin, and Kim Nguyen for assistance in synthesis and refolding of bass hepcidin, and Shenggen Yao for assistance in collecting NMR spectra.

REFERENCES

1. Krause, A., Neitz, S., Magert, H. J., Schulz, A., Forssmann, W. G., Schulz-Knappe, P., and Adermann, K. (2000) *FEBS Lett.* **480,** 147–150
2. Park, C. H., Valore, E. V., Waring, A. J., and Ganz, T. (2001) *J. Biol. Chem.* **276,** 7806–7810
3. Ganz, T. (2003) *Blood* **102,** 783–788
4. Hunter, H. N., Fulton, D. B., Ganz, T., and Vogel, H. J. (2002) *J. Biol. Chem.* **277,** 37597–37603
5. Lauth, X., Shike, H., Burns, J. C., Westerman, M. E., Ostland, V. E., Carlberg, J. M., Van Olst, J. C., Nizet, V., Taylor, S. W., Shimizu, C., and Bulet, P. (2002) *J. Biol. Chem.* **277,** 5030–5039
6. Shike, H., Lauth, X., Westerman, M. E., Ostland, V. E., Carlberg, J. M., Van Olst, J. C., Shimizu, C., Bulet, P., and Burns, J. C. (2002) *Eur. J. Biochem.* **269,** 2232–2237
7. Pigeon, C., Ilyin, G., Courselaud, B., Leroyer, P., Turlin, B., Brissot, P., and Loreal, O. (2001) *J. Biol. Chem.* **276,** 7811–7819
8. Nicolas, G., Bennoun, M., Devaux, I., Beaumont, C., Grandchamp, B., Kahn, A., and Vaulont, S. (2001) *Proc. Natl. Acad. Sci. U. S. A.* **98,** 8780–8785
9. Nicolas, G., Bennoun, M., Porteu, A., Mativet, S., Beaumont, C., Grandchamp, B., Sirito, M., Sawadogo, M., Kahn, A., and Vaulont, S. (2002) *Proc. Natl. Acad. Sci. U. S. A.* **99,** 4596–4601
10. Fleming, R. E., and Sly, W. S. (2001) *Proc. Natl. Acad. Sci. U. S. A.* **98,** 8160–8162
11. Roetto, A., Papanikolaou, G., Politou, M., Alberti, F., Girelli, D., Christakis, J., Loukopoulos, D., and Camaschella, C. (2003) *Nat. Genet.* **33,** 21–22
12. Delatycki, M., Allen, K., Gow, P., MacFarlane, J., Radomski, C., Thompson, J., Hayden, M., Goldberg, Y., and Samuels, M. (2004) *Clin. Genet.* **65,** 378–383
13. Pietrangelo, A. (2004) *N. Engl. J. Med.* **350,** 2383–2397
14. Nicolas, G., Chauvet, C., Viatte, L., Danan, J. L., Bigard, X., Devaux, I., Beaumont, C., Kahn, A., and Vaulont, S. (2002) *J. Clin. Investig.* **110,** 1037–1044
15. Anderson, G. J., Frazer, D. M., Wilkins, S. J., Becker, E. M., Millard, K. N., Murphy, T. L., McKie, A. T., and Vulpe, C. D. (2002) *Biochem. Soc. Trans.* **30,** 724–726
16. Nemeth, E., Valore, E. V., Territo, M., Schiller, G., Lichtenstein, A., and Ganz, T. (2003) *Blood* **101,** 2461–2463
17. Nemeth, E., Rivera, S., Gabayan, V., Keller, C., Taudorf, S., Pedersen, B. K., and Ganz, T. (2004) *J. Clin. Investig.* **113,** 1271–1276
18. Kaiser, E., Colescott, R. L., Bossinger, C. D., and Cook, P. I. (1970) *Anal. Biochem.* **34,** 595–598
19. King, D. S., Fields, C. G., and Fields, G. B. (1990) *Int. J. Pept. Protein Res.* **36,** 255–266
20. Rivier, J., and McClintock, R. (1983) *J. Chromatogr.* **268,** 112–119
21. Sklenar, V., Piotto, M., Leppik, R., and Saudek, V. (1993) *J. Magn. Reson.* **102,** 241–245
22. Delaglio, F., Grzesiek, S., Vuister, G. W., Zhu, G., Pfeifer, J., and Bax, A. (1995) *J. Biomol. NMR* **6,** 277–293
23. Bartels, C., Xia, T.-H., Güntert, P., and Wüthrich, K. (1995) *J. Biomol. NMR* **6,** 1–10
24. Barnham, K. J., Monks, S. A., Hinds, M. G., Azad, A. A., and Norton, R. S. (1997) *Biochemistry* **36,** 5970–5980
25. Cornilescu, G., Delaglio, F., and Bax, A. (1999) *J. Biomol. NMR* **13,** 289–302
26. Dingley, A. J., Mackay, J. P., Chapman, B. E., Morris, M. B., Kuchel, P. W., Hambly, B. D., and King, G. F. (1995) *J. Biomol. NMR* **6,** 321–328
27. Yao, S., Howlett, G. J., and Norton, R. S. (2000) *J. Biomol. NMR* **16,** 109–119
28. Herrmann, T., Guntert, P., and Wüthrich, K. (2002) *J. Mol. Biol.* **319,** 209–227
29. Linge, J. P., and Nilges, M. (1999) *J. Biomol. NMR* **13,** 51–59
30. Koradi, R., Billeter, M., and Wüthrich, K. (1996) *J. Mol. Graphics* **14,** 51–55
31. Laskowski, R. A., Rullmannn, J. A., MacArthur, M. W., Kaptein, R., and Thornton, J. M. (1996) *J. Biomol. NMR* **8,** 477–486
32. Berman, H. M., Westbrook, J., Feng, Z., Gilliland, G., Bhat, T. N., Weissig, H., Shindyalov, I. N., and Bourne, P. E. (2000) *Nucleic Acids Res.* **28,** 235–242
33. Hetru, C., and Bulet, P. (1997) *Methods Mol. Biol.* **78,** 35–49
34. Casteels, P., Ampe, C., Jacobs, F., and Tempst, P. (1993) *J. Biol. Chem.* **268,** 7044–7054
35. Berenbaum, M. (1981) *Adv. Cancer Res.* **35,** 269–335
36. Broekaert, W. F., Terras, F. R., Cammue, B. P., and Osborn, R. W. (1995) *Plant Physiol.* **108,** 1353–1358
37. Borriello, F., and Lederer, J. (1995) *BioTechniques* **19,** 580–584
38. Auboeuf, D., and Vidal, H. (1997) *Anal. Biochem.* **245,** 141–148
39. Tam, J. P., Wu, C. R., Liu, W., and Zhang, J. W. (1991) *J. Am. Chem. Soc.* **113,** 6657–6662
40. Carugo, O., Cemazar, M., Zahariev, S., Hudaky, I., Gaspari, Z., Perczel, A., and Pongor, S. (2003) *Protein Eng.* **16,** 637–639
41. Amsterdam, D. (1996) in *Antibiotics in Laboratory Medicine* (Lorean, V., ed) 4th Ed., pp. 52–111, Williams & Wilkins, Baltimore
42. Tossi, A., Sandri, L., and Giangaspero, A. (2000) *Biopolymers* **55,** 4–30
43. Laederach, A., Andreotti, A. H., and Fulton, D. B. (2002) *Biochemistry* **41,** 12359–12368
44. Mandard, N., Bulet, P., Caille, A., Daffre, S., and Vovelle, F. (2002) *Eur. J. Biochem.* **269,** 1190–1198
45. Mandard, N., Sodano, P., Labbe, H., Bonmatin, J. M., Bulet, P., Hetru, C., Ptak, M., and Vovelle, F. (1998) *Eur. J. Biochem.* **256,** 404–410
46. Trabi, M., Schirra, H. J., and Craik, D. J. (2001) *Biochemistry* **40,** 4211–4221
47. Hwang, P. M., Zhou, N., Shan, X., Arrowsmith, C. H., and Vogel, H. J. (1998) *Biochemistry* **37,** 4288–4298
48. Wang, X., Connor, M., Smith, R., Maciejewski, M. W., Howden, M. E., Nicholson, G. M., Christie, M. J., and King, G. F. (2000) *Nat. Struct. Biol.* **7,** 505–513
49. Xia, Z. X., He, Y. N., Dai, W. W., White, S. A., Boyd, G. D., and Mathews, F. S. (1999) *Biochemistry* **38,** 1214–1220
50. Blake, C. C., Ghosh, M., Harlos, K., Avezoux, A., and Anthony, C. (1994) *Nat. Struct. Biol.* **1,** 102–105
51. Czajkowski, C., and Karlin, A. (1995) *J. Biol. Chem.* **270,** 3160–3164
52. Engst, S., and Miller, S. M. (1999) *Biochemistry* **38,** 3519–3529
53. Hancock, R. E. W., and Chapple, D. S. (1999) *Antimicrob. Agents Chemother.* **43,** 1317–1323
54. Zhang, L., Dhillon, P., Yan, H., Farmer, S., and Hancock, R. E. (2000) *Antimicrob. Agents Chemother.* **44,** 3317–3321
55. Saint, N., Cadiou, H., Bessin, Y., and Molle, G. (2002) *Biochim. Biophys. Acta* **1564,** 359–364
56. Shai, Y. (2002) *Biopolymers* **66,** 236–248
57. Powers, J. P., and Hancock, R. E. (2003) *Peptides* **24,** 1681–1691
58. Bengoechea, J. A., and Skurnik, M. (2000) *Mol. Microbiol.* **37,** 67–80
59. Ganz, T. (2002) *Isr. Med. Assoc. J.* **4,** 1043–1045
60. Yan, H., and Hancock, R. E. (2001) *Antimicrob. Agents Chemother.* **45,** 1558–1560
61. Patrzykat, A., Zhang, L., Mendoza, V., Iwama, G. K., and Hancock, R. E. (2001) *Antimicrob. Agents Chemother.* **45,** 1337–1342
62. Mor, A., Hani, K., and Nicolas, P. (1994) *J. Biol. Chem.* **269,** 31635–31641
63. Silphaduang, U., and Noga, E. J. (2001) *Nature* **414,** 268–269
64. Jurado, R. L. (1997) *Clin. Infect. Dis.* **25,** 888–895
65. Ashrafian, H. (2003) *Infect. Immun.* **71,** 6693–6700
66. Congleton, J. L., and Wagner, E. J. (1991) *Comp. Biochem. Physiol. A* **98,** 195–200
67. Langston, A. L., Johnstone, R., and Ellis, A. E. (2001) *Fish Shellfish Immunol.* **11,** 333–345
68. Chen, M. F., Yun, S., Marty, G. D., McDowell, T. S., House, M. L., Appersen, J. A., Guenther, T. A., Arkush, K. D., and Hedrick, R. P. (2000) *Dis. Aquat. Org.* **43,** 117–126
69. Nicholls, A., Sharp, K. A., and Honig, B. (1991) *Proteins* **11,** 281–296